Journal of Applied Electrochemistry **32**: 831–838, 2002.

Chlorine evolution in a centrifugal field

H. CHENG, K. SCOTT* and C. RAMSHAW
Department of Chemical & Process Engineering, University of Newcastle upon Tyne, Newcastle upon Tyne, NE1 7RU, Great Britain
*(*author for correspondence, fax: +44 0191 222 5292, e-mail: k.scott@ncl.ac.uk)*

Received 2 October 2001; accepted in revised form 10 April 2002

Key words: centrifugal fields, chlorine evolution, chlor-alkali cell, process intensification

Abstract

Intensification of the electrochemical production of chlorine and sodium hydroxide (i.e., the chlor-alkali process) was demonstrated in a centrifugal acceleration field. This intensification was shown by comparing the cell voltages and the anode potentials for a cell operated with and without a centrifugal field applied using the linear sweep voltammetric, galvanostatic and potentiostatic polarizations. Under industrial chlor-alkali electrolysis conditions, a cell voltage reduction of up to 600 mV and an anode potential reduction of up to 360 mV at 600 mA cm^{-2} were achieved by using a relative acceleration rate of 190 *g* with an acidic saturated NaCl solution at 80 °C. The relationships between the cell performance and relative acceleration rate, for different anode materials, temperature and NaCl concentration are reported.

1. Introduction

Chlor-alkali production is the largest scale industrial electrosynthesis; a rate of $3.5 \sim 4.0 \times 10^7$ tons Cl_2 per year world-wide [1, 2]. The progress in chlor-alkali technology has been reviewed extensively (e.g., [2–11]). Under typical operating conditions the reversible potentials are, at the anode 1.247 V (versus reversible hydrogen electrode, RHE), at the cathode −0.797 V vs RHE, giving a total reversible cell voltage of 2.23 V [12]. At the current densities used (i.e., 1–5 kA m^{-2}) one of the major issues confronting the chlor-alkali industry is the high power consumption, about 10^8 MWh of electricity per year [2]. It was estimated that the power consumption accounts for over 50% of the operating costs [13, 14].

Significant improvement of the electrolytic process in this aspect (i.e., reduction in cell voltage) would be beneficial, both economically and environmentally. This means that 90% of the total reduction in cell voltage is due to certain properties that may not be directly related to the electrocatalytic properties. Chlor-alkali electrolysis involves the generation of gases at both of the electrodes, for example, chlorine evolution at the anode and hydrogen evolution at the cathode. This can introduce a relatively high resistance of the cell due to severe gas blanketing of the electrodes and the membrane and poor conductivity of the bubble-filled electrolytes. Both effects incur significant overvoltage, for example, about 0.4 V at a current density of 300 mA cm^{-2} in ICI electrolysers (FM21 units) [16]. Therefore, it is important to try and ensure efficient gas disengagement from the electrolyte, the electrodes and any intervening diaphragm/membrane, in the operation of chlor-alkali cells [16].

Gas disengagement can be achieved in various ways, such as pumping electrolyte through the electrochemical cell or using moving electrodes. However, such methods enhance mass transfer and eliminate bubble effect to a limited extent. For example, the rotating cylinder electrode may be used [17] but enhancement in mass transfer to a rotating cylinder electrode depends to a large extent upon microturbulence at the electrode surface and is at the expense of high shear losses. One option for intensification is to design equipment wherein the electrolyte is subjected to a centrifugal force to promote good mass transport within the cell and the separation of gas bubbles from the electrodes, the electrolytes and the membrane. This approach is an attractive strategy in the chemical industry and was pioneered in ICI during the late 1970s [16].

Process intensification is in principle particularly attractive for electrochemical processes that are, typically, multiphase systems. When a centrifugal field is applied to a multiphase system, the light phase (e.g., gas) will flow inward, whereas the centrifugal effect will tend to sweep the denser fluid outward. In a cell this would give a rapid and efficient removal of the electrolytic gas from the interelectrode gap. The interphase buoyancy force determines the fluid dynamics of multiphase systems and because this force is large in a centrifugal field, droplets and/or bubbles will be small and the

interphase slip velocity will be high [16]. Moreover, bubbles disengagement from the electrodes, electrolytes, membranes, and the interelectrode area would be greatly facilitated in a centrifugal field; greatly reducing gas blanketing, thereby making significant reductions in the cell voltage. The idea was demonstrated by preliminary work at ICI with a rotating chlor-alkali membrane cell [16]. When operated under similar conditions to those encountered in a commercial ICI cell (FM21), very significant overall voltage savings were achieved in centrifugal fields. For example, at a relative acceleration rate (denoted as g) of 25, the overall cell voltage was 2.85 V at 300 mA cm^{-2}, which was much lower than the 3.17 V obtained in ICI FM21 cells [16].

The present work was undertaken to investigate the behaviour of a chlor-alkali cell in a simple laboratory centrifuge, in order to provide data on the effect of process conditions and centrifugal acceleration on cell performance. An objective of the research was to assess whether the performance benefit of centrifugal fields could justify the additional cost of operating a bipolar array of cells in a rotor. It should be noted in this context that the energy needed to rotate the cell and overcome windage, friction etc., will be quite small compared to that which could be saved. For example, a 100 kA cell operating with a bubble overvoltage of 0.3 V has a potential energy saving of approximately 30 kW whereas the equipment rotor (1 m long $\times$ 0.5 m dia.) will require approximately 2 kW to rotate at around 700 rpm.

2. Experimental details

2.1. *Centrifugal rig and cell*

Experiments were carried out in a laboratory centrifugal rig (Figure 1), with a two-compartment batch membrane cell, of 50 cm^3 capacity (Figure 2). The cell was used to evaluate the influence of centrifugal fields on gas evolution reactions and not as a prototype chlor-alkali reactor.

The membrane cell (detailed later) was housed in an MSE Super Minor Centrifuge (England). To achieve high temperature cell operation, heated (using 200 W barrel heaters) compressed air was introduced into the centrifuge. A thermocouple was used to determine the temperature of the outlet air. The system was heated for 20 min before electrochemical measurements and the hot air was passed through the centrifuge pool during the experiments. The cell and its counter balance (i.e., a duplicate cell) were connected to the axis of the centrifuge using stainless steel rods. The cell under the influence of a centrifugal field (i.e., rotating) was positioned horizontally and when stationary (i.e., not rotating) it was positioned vertically.

Figure 2(a) and (b) show the side view and cross-sectional view of the cell. The cell consisted of polyethylene blocks, each with internal volumes of 50 ml. The

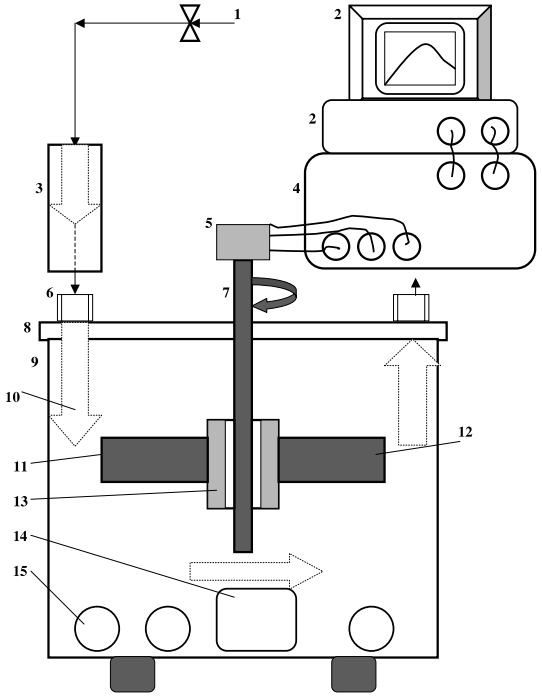

Fig. 1. Side view of the centrifugal rig. Key: (1) compressed air, (2) computer, (3) air heater, (4) potentiostat, (5) slip ring, (6) inlet or outlet of hot air, (7) axis, (8) cover of the centrifuge, (9) centrifuge, (10) hot air, (11) cell, (12) counter part of the cell, (13) stainless steel rods and fixed caps and screws, (14) revolution meter and (15) controls.

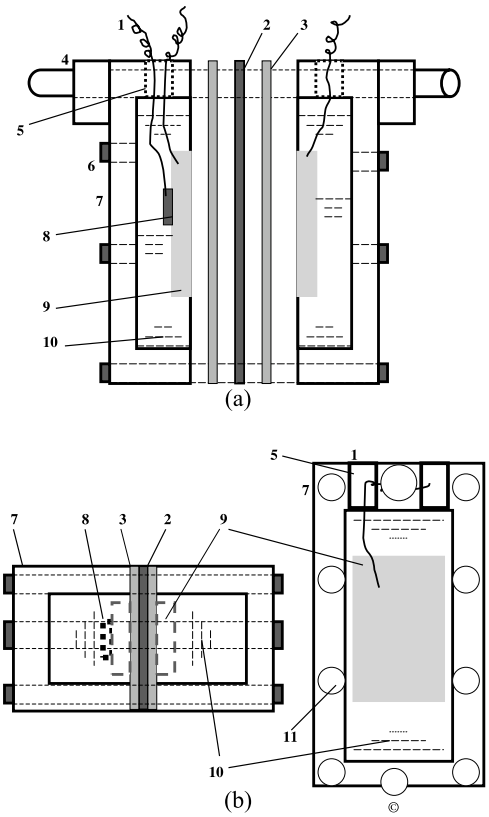

Fig. 2. Details of the rotary cell: (a) side view and (b) cross-sectional view (top). (c) Cross-sectional view of the electrode chamber. Key: (1) connection wires, (2) membrane, (3) gaskets (4) stainless steel rods, (5) holes for discharging of gas and electrolytes, (6) bolts and screws, (7) polypropylene block, (8) reference electrode, (9) working and counter electrodes, (10) electrolytes and (11) holes for the bolts and screws.

electrode was held between two electrically conducting meshes (usually made up of expanded Pt/Ti metal) in electrolyte 'channels'. Working and counter electrode chambers were separated by a membrane (Nafion® 117, DuPont). The cell was held together between two blocks using a set of retaining bolts positioned around the periphery of the cell and sealed with silicon rubber gaskets. Figure 2(c) details the cross-sectional views of the working and counter chambers. Other details of the rig and cells are described elsewhere [18].

The RuO_2–TiO_2/Ti mesh and Pt/Ti mesh electrodes used in this work were prepared, by thermal oxidation, according to published methods [11, 19–21] and detailed elsewhere [18]. The 'electrode area' used to calculate the current density is the overall electrode area projected onto the membrane. The reference electrode used to measure the anode potential was made of Nafion® membrane (DuPont), which was placed near the working electrode and connected to the potentiostat through a stainless steel wire. The reference electrode was regularly calibrated against a saturated calomel reference electrode. All electrode potentials are quoted against the reversible hydrogen electrode (RHE). Other details of this reference electrode are reported elsewhere [18].

2.2. *Electrochemical measurements*

The polarization behaviour of the cell was investigated using a model 273 EG&G Princeton potentiostat/galvanostat controlled with M270/250 electrochemistry software (version 4.11). Three electrochemical methods were used; linear sweep voltammetry, galvanostatic polarization and potentiostatic polarizations. Linear sweep voltammetry was employed in most of the work described in this paper for the evaluation of electrodes and the effects of centrifugal fields. To obtain quasi-steady-state polarization data, a scan rate of 5 mV s^{-1} was used throughout this work, as the results obtained using 1 mV s^{-1} typically showed the same features as those at 5 mV s^{-1}. In galvanostatic polarization a current was applied to the working electrode and the potential monitored until it remained constant for a specified time (5–10 min) and then the resulting potential was recorded. The electrode polarization was measured at current densities of 0, 0.1, 0.5, 1, 2, 3 or 400 mA cm^{-2} for most temperatures and reactant concentrations. In potentiostatic polarization measurements, constant electrode potentials were applied to the electrodes, and the current density of the electrode recorded as a function of time. The applied electrode potentials were chosen according to electrode material, temperature and reactant concentration and generally ranged from open circuit potential to 3.5 V vs RHE for the anode.

Electrolyte solutions were prepared from Analar grade NaCl, NaOH, and HCl (BDH) and de-ionized (Millipore) water. Most experiments used NaCl solutions as the electrolytes. To examine the effect of NaCl concentration, the following solutions were used: 0.5 mol dm^{-3} (M) (pH 6.51), 1 M (pH 7.05), 2 M (pH 7.30), 4 M (pH 7.38) and saturated (approximately 6.2 M at the ambient temperature, pH 8.24). All measurements were repeated with fresh solutions at least twice under the same conditions to ensure reproducibility. The change in electrolyte composition was negligible over the duration of each experiment.

3. Results and discussion

Preliminary screening of the following electrode materials was undertaken to identify anodes with good chlorine evolution polarization characteristics: a carbon cloth (GC-14, E-Tek), a carbon fibre paper (PC 206, Stackpole) with a thickness of 0.5 mm, a carbon fibre felt (SPC 7011, SIGRATEX Carbon Group) with a thickness of 8 mm, a platinum/titanium expanded metal, a TYSAR™ EP, a platinized titanium fibre mat (The Electrosynthesis Co., USA), a dimensionally stable anode (DSA), with a thickness of about 0.5 mm, and the RuO_2–TiO_2/Ti electrode. Of these materials the DSA and RuO_2–TiO_2/Ti mesh anode gave the better polarization performances [18]. The effect of ruthenium content in the latter electrode was also examined and a loading of 2 mg Ru cm^{-2} was found to give good performance and was selected for subsequent tests. For example with a ruthenium content of 2 mg Ru cm^{-2}, at a relative acceleration rate of 190 *g*, a current density of 400 mA cm^{-2} was achieved at approximately 2.10 V vs RHE. This was approximately 0.3 V lower than that obtained with the commercial DSA anode. In the case of the RuO_2–TiO_2/Ti anode the Ti mesh substrate had a fine structure (mesh open area 37% and wire diameter 0.25 mm opening) and provided a high active surface area of catalyst compared to the DSA anode, which had a Ti expanded metal substrate.

3.1. *Relative acceleration rate*

The data reported in this paper were obtained in a relatively simple chlor-alkali cell, with a stationary pool of electrolyte, far from being optimised to reduce cell voltage for chlorine evolution reaction. Thus the focus of the work was to assess the impact of the application of centrifugal fields on the cell voltage and anode potential.

3.1.1. *Effect on cell voltage*

Figure 3 shows cell voltage/current density curves obtained from the chlor-alkali cell, with a RuO_2–TiO_2/Ti mesh anode, operated in centrifugal fields or stationary at 80 °C. The relative acceleration rate affects cell polarization behaviour significantly, especially at higher current densities (i.e., cell voltage reduction) is more significant at higher current densities.

The reduction in cell voltage obtained in centrifugal fields is shown in Figure 4 as a function of relative

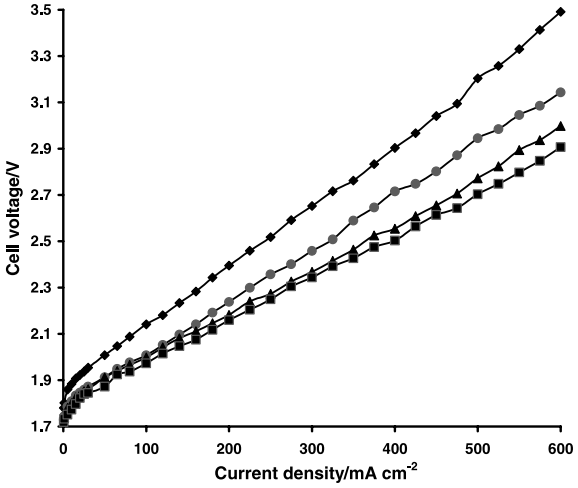

Fig. 3. Representative cell voltage against current density curves for Cl_2 evolution reaction in centrifugal fields. Anode: RuO_2/Ti mesh (2 mg Ru cm^{-2}). Cathode: Pt/Ti mesh (2 mg Pt cm^{-2}). Anolyte: 0.5 M HCl + saturated NaCl solution. Catholyte: 10% NaOH solution. Scan rate 5 mV s^{-1}. Temperature: 80 °C. Relative acceleration rate: (♦) 1 *g*, (●) 25 *g*, (▲) 100 *g* and (■) 190 *g*.

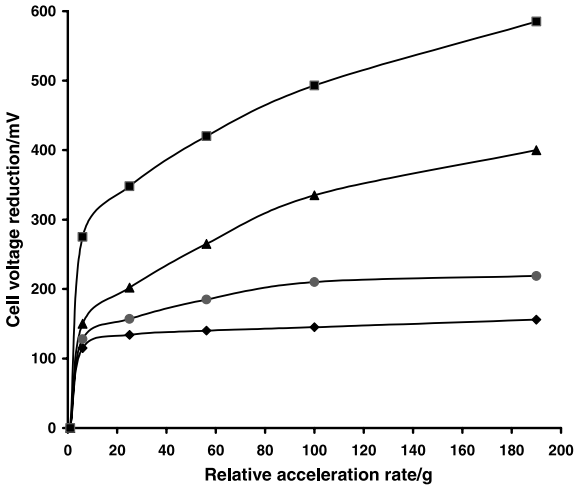

Fig. 4. Cell voltage reduction of chlor-alkali cell as a function of relative acceleration rate at various current densities. Current density: (♦) 100, (●) 200, (▲) 400 and (■) 600 mA cm^{-2}. Other conditions as in Figure 3.

acceleration rate where the uncompensated solution resistances have been corrected. The data were collected with the RuO_2–TiO_2/Ti anode at a scan rate of 5 mV s^{-1}. At all current densities, the magnitude of voltage reduction increased rapidly from 1 *g* to about 25 *g*, after which its rate of increase slowed (Figure 4). The highest reduction in cell voltage, 600 mV, was achieved at 190 *g* and a current density of 600 mA cm^{-2}. These observations are not surprising as the overall rate of the chlorine evolution reaction is strongly influenced by slow transfer of Cl_2 away from the interface [22]. Under intensive gas evolution on the electrode, mass transfer of the reaction product into the bulk solution is strongly affected by the convection fluxes existing near the electrode surface. This is determined not only by the disengagement and removal of the gas bubbles from the surface, but also by their growth at the surface and, after their break-off, in the solution at the vicinity of the electrode [23–27]. At relatively low current densities, gas product removal proceeds mainly through diffusion of the reaction product molecules into the bulk solution, whilst at high current densities, under supersaturation of the electrode solution layer by the reaction product, its removal would preferentially go through gas evolution. The electrode chambers will therefore be filled with gas-electrolyte mixtures [27]. In industrial practice the cells operate typically at approximately 90 °C at which temperature the water partial pressure is relatively high (~68 kPa). This results in a larger volumetric flux of gas/vapour from an electrode operating at a given current density and makes the electrode more susceptible to gas blinding. Thus bubbles will be more efficiently removed from the electrode surfaces and the membrane by centrifugal acceleration due to its function of disengaging gas bubbles. This, in turn, will reduce the cell resistance drastically.

3.1.2. *Anode potential*

The effect of centrifugal fields on the anode potential for a RuO_2–TiO_2/Ti mesh anode is shown in Figure 5. Anode potential decreased rapidly, at a given current density, with increased relative acceleration rate, particularly at high current densities. For example, at 600 mA cm^{-2}, anode potentials were 2.10, 1.71 and 1.58 V vs RHE at 1, 100 and 190 *g*, respectively. Evidently, the centrifugal field promoted high interphase slip velocity and, therefore, enhanced mass transport and gas disengagement. This increased the supply of the reactants to the electrode, increased the active electrode area and thus decreased the anode potential.

The effect of relative acceleration rate on the reduction in anode potential is shown in Figure 6. Data were obtained by linear sweep voltammetry at a scan rate of

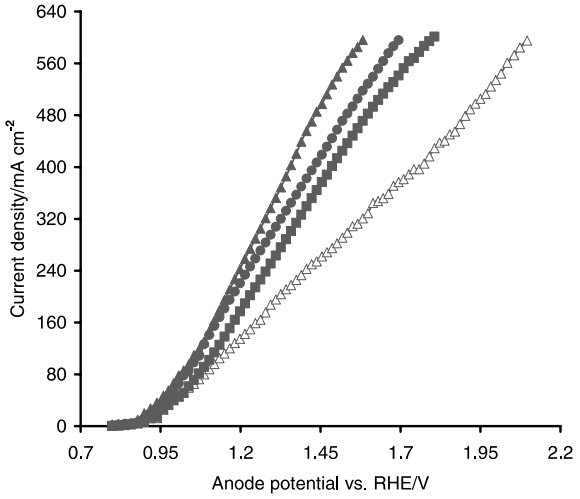

Fig. 5. Anode polarization curves for Cl_2 evolution reaction in centrifugal fields. Conditions as in Figure 3. Relative acceleration rate: (△) 1 *g*, (■) 25 *g*, (●) 100 *g* and (▲) 190 *g*.

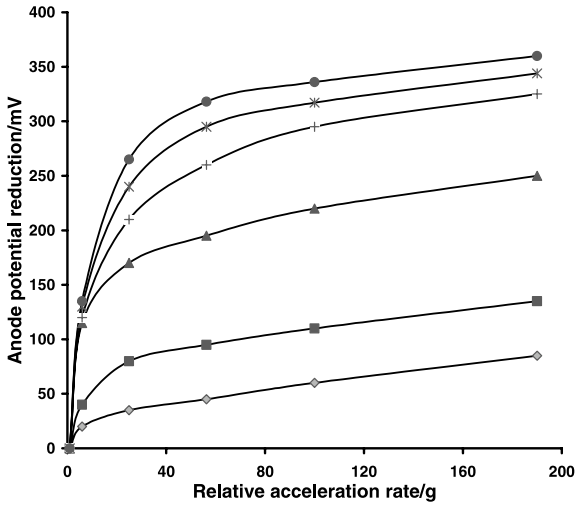

Fig. 6. Anode potential reduction of chlor-alkali cell as a function of relative acceleration rate at various current densities. Other conditions as in Figure 3. Current density: (♦) 100, (■) 200, (▲) 300, (+) 400, (∗) 500 and (●) 600 mA cm^{-2}.

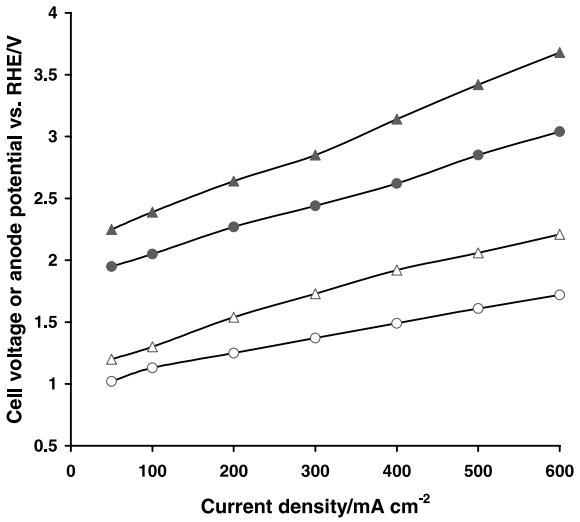

Fig. 7. Steady-state anode and cell polarization curves of chlor-alkali cell in two types of electrolytes at a relative acceleration rate of 190 *g* and 80 °C. Electrolyte A: use 6.2 mol dm^{-3} NaCl as both anolyte and catholyte. Electrolyte B: use 0.5 mol dm^{-3} HCl plus 6.2 mol dm^{-3} NaCl as anolyte and 10% NaOH as catholyte. Data collection method: chronoamperometry. Anode potential: (△) electrolyte A; (○) electrolyte B. Cell voltage: (▲) electrolyte A; (●) electrolyte B.

5 mV s^{-1}. A significant reduction in anode potential, of 360 mV, was achieved at a current density of 600 mA cm^{-2} at 190 *g*. The reduction in anode potential was much lower at low current density and only small differences in potential were observed at lower values of *g*. It was also not possible to correct for the IR voltage drops for the anode and the cathode respectively during the data analyses because of special structures of the electrodes. Since the reference electrode was close to the working electrode in our measurements, the uncompensated resistances between the working electrodes and the reference electrode should be a small fraction of the total resistance [33].

3.2. *Effect of electrolyte*

The performance of chlor-alkali cells can be improved by adding hydrochloric acid to the NaCl feed as this increases chlorine purity by reducing oxygen discharge at the anode [28]. Figure 7 compares typical steady-state polarization curves for the chlor-alkali cell and/or the RuO_2/Ti mesh anode only. The curves were obtained in two types of electrolytes: type A, 6.2 mol dm^{-3} NaCl as both anolyte and catholyte; and type B, 0.5 mol dm^{-3} HCl in 6.2 mol dm^{-3} NaCl as anolyte and 10% NaOH as catholyte. The curves were collected by chronoamperometric measurements at 190 *g* and 80 °C. It can be seen, from Figure 7, that in a centrifugal field, both anode potential and cell voltage were lower, at a constant current density, when the acidified anolyte and the alkaline catholyte were used rather than the saturated NaCl electrolytes. For example, at an acceleration rate of 190 *g* and a current density of 100 mA cm^{-2}, the anode potentials were 1.13 and 1.30 V vs RHE and the cell voltages were 2.10 and 2.48 V for the acidified anolyte and the saturated NaCl electrolytes, respectively. At higher current densities, the differences in potential were more significant. For example, at 600 mA cm^{-2} and an acceleration rate of 190 *g*, an anode potential reduction of about 0.49 V and a cell voltage reduction of about 0.84 V were achieved by using the acidified anolyte rather than the saturated NaCl electrolytes.

3.3. *NaCl concentration*

It is well known that the relatively low oxygen overpotentials of metal oxide electrodes in chlor-alkali cells reduce the current efficiency for the Cl_2 generation as a result of parasitic generation of oxygen [29]. Current efficiencies for the Cl_2 evolution are higher in more concentrated solutions: >99% in 4 M NaCl and >92% in 0.4 M NaCl solution [30, 31].

The effect of NaCl concentration on the cell voltage, using a chlor-alkali cell with DSA anodes, is shown in Figure 8. Data were obtained at a relative acceleration rate of 190 *g* and at ambient temperature using linear sweep voltammetry at a scan rate of 5 mV s^{-1}. The uncompensated solution resistances have been corrected during the data analyses. As expected, current density rises with increase in NaCl concentration, at a fixed cell voltage. This effect is due mainly to an increase in conductivity of the electrolyte and to a lesser extent reduction in decomposition potential with increase in reactant concentration.

The reduction in cell voltage, which directly reflects the effect of centrifugal fields, also showed a strong dependence on the NaCl concentrations (Figure 9). The data were collected from a chlor-alkali cell, with a DSA anode, operated in both centrifugal and gravitational fields, by linear sweep voltammetry at a scan rate of

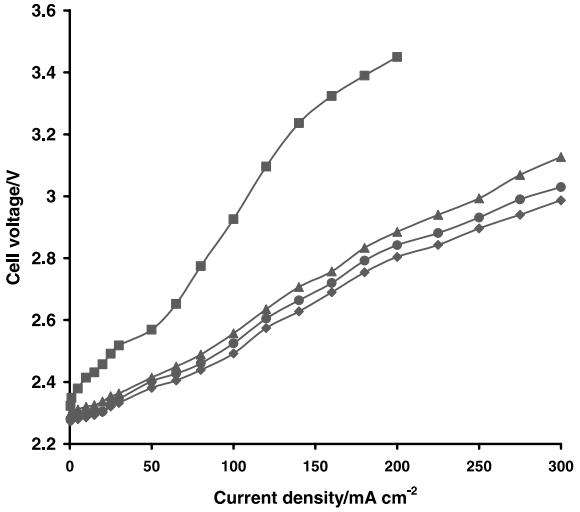

Fig. 8. Effect of reactant concentration on polarization behaviour of chlor-alkali cell at a relative acceleration rate of 190 *g*. Anode: DSA. Anolyte concentration: (♦) 6.2, (●) 4.0, (▲) 2.0 and (■) 0.5 M NaCl. Catholyte: 10% NaOH. Other conditions as in Figure 3.

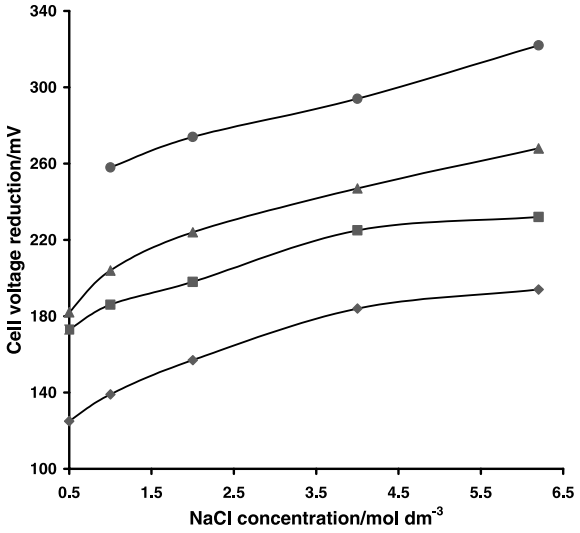

Fig. 9. Effect of reactant concentration on chlor-alkali cell voltage reduction ($E_{\text{cell},1\,g} - E_{\text{cell},190\,g}$) at different current densities. Other conditions as in Figure 8. Current density: (♦) 50, (■) 100, (▲) 200 and (●) 300 mA cm^{-2}.

5 mV s^{-1}. As shown in Figure 9, at a fixed current density, the cell voltage reduction increased rapidly when the NaCl concentration was increased from 0.5 to 1 M and then increased at a slower rate with a further increase in concentration. More significant cell voltage reductions were achieved in concentrated solutions at higher operating current densities: for example, at ambient temperature, 110 mV in 0.5 mol dm^{-3} NaCl solution at 50 mA cm^{-2}, compared with 285 mV in 6.2 mol dm^{-3} NaCl solution at 300 mA cm^{-2}.

The effect of an increase in NaCl concentration on anode potential exhibited a similar trend as that for cell voltage. For example, at 190 *g*, ambient temperature

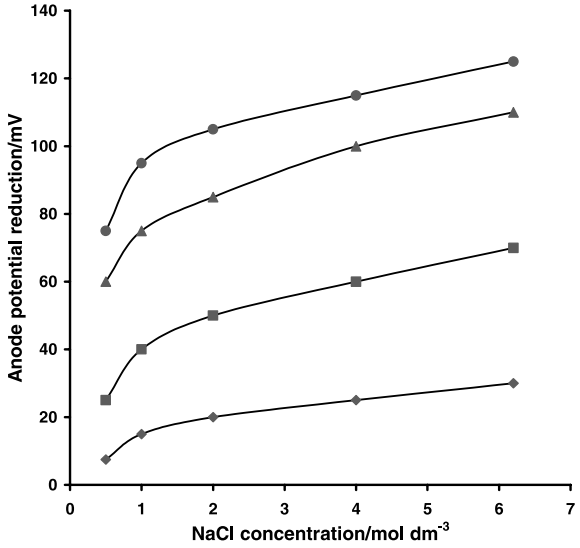

Fig. 10. Effect of reactant concentration on anode potential reduction of chlor-alkali cell at a relative acceleration rate of 190 *g* and 80 °C. Anode: DSA. Data collection method: galvanostatic measurements. Other conditions as in Figure 3. Current density: (♦) 50, (■) 100, (▲) 200 and (●) 300 mA cm^{-2}.

and an anode potential of 1.7 V vs RHE, current density increased from 80 mA cm^{-2} with 0.5 mol dm^{-3} NaCl solution to 325 mA cm^{-2} with 6.2 mol dm^{-3} NaCl solutions. The effect of the centrifugal field on the reduction in anode potential, at different NaCl concentrations, for DSA, is shown in Figure 10. Data were obtained by galvanostatic polarization and no IR compensation was made due to the technical difficulties mentioned previously. The reduction in anode potential varied significantly with current density and was small at low current density: for example, only 10 mV in 0.5 mol dm^{-3} NaCl solution at 50 mA cm^{-2}.

It is evident that the centrifugal fields not only reduced mass transport limitation but also assisted bubble disengagement from the electrode surface; both factors intensified the concentration effect in centrifugal fields. An increase of mass transfer coefficients, from 1.28×10^{-5} m s^{-1} to 3.89×10^{-4} m s^{-1} when the relative acceleration rate increased from 1 to 190 *g*, were observed [32]. However, it should be stated that the superior performance in the concentrated NaCl solutions was predominantly due to a decrease in ohmic resistance of the cell, even in centrifugal fields. For example, from the experiments presented in Figure 8, at 190 *g* and 100 mA cm^{-2}, solution IR drop is estimated to have decreased from 0.42 to 0.165 V on increasing the NaCl concentration from 0.5 to 6.2 mol dm^{-3}. Generally, it is worthwhile to measure the IR voltage drop and thus to distinguish the effect of centrifugal field on various aspects, for example, solution conductivity and mass transfer. Although such measurements are impossible under the present conditions, the above data demonstrate qualitatively that centrifugal fields greatly affect both IR drop and mass transfer, even in a laboratory-scale rotary cell.

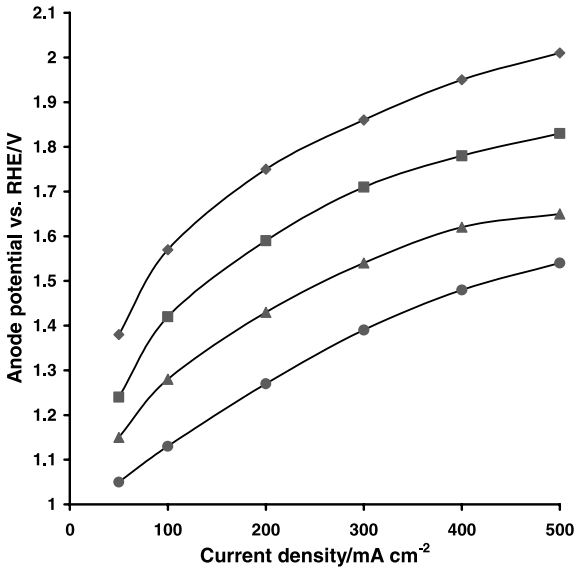

Fig. 11. Effect of temperature on anode polarization curves for Cl_2 evolution reaction at a relative acceleration rate of 190 *g*. Other conditions as in Figure 3. Temperature: (♦) 25, (■) 40, (▲) 60 and (●) 80 °C.

3.4. *Effect of temperature*

An increase in cell temperature has a beneficial effect on the anode potential as shown in Figures 11 and 12. Again, the uncompensated resistance between the anode and the reference electrode was not corrected because of the technical difficulties mentioned previously. The data shown in Figure 11 were obtained from steady-state measurements using potentiostatic polarization technique in a chlor-alkali cell with the RuO_2/Ti mesh anode at several temperatures and a relative acceleration rate of 190 *g*.

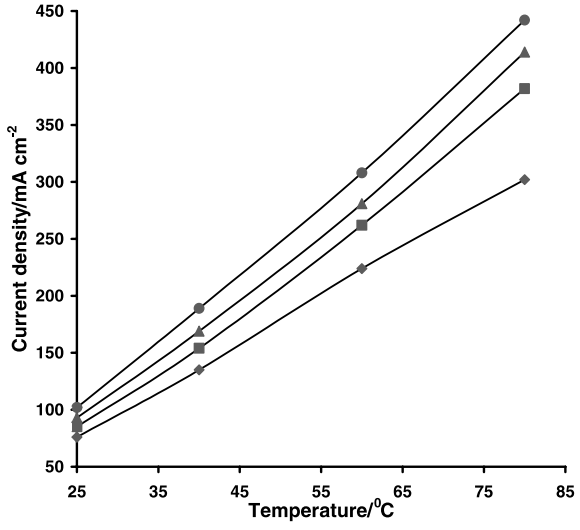

Fig. 12. Effect of temperature on anode current density of chlor-alkali cell at different relative acceleration rates. Data collection method: chronoamperometry (at 1.5 V vs RHE). Relative acceleration rate: (♦) 1 *g*, (■) 25 *g*, (▲) 100 *g* and (●) 190 *g*. Other conditions as in Figure 3.

The anode potential, at a constant current density, decreased with an increase in cell temperature (Figure 11): for example, at 300 mA cm^{-2}, from 1.86 V vs RHE at 25 °C to 1.39 V vs RHE at 80 °C. The current density increased faster with increase in temperature in the centrifugal fields, as indicated in Figure 12, at an anode potential of 1.5 V vs RHE. The rate is 61.8 A m^{-2} per °C at 190 *g*, compared with 41.1 A m^{-2} per °C, obtained at 1 *g*. The cell voltage was similarly affected by an increase in temperature. For example, when the temperature was increased from 25 °C to 80 °C, the cell voltage decreased by approximately 250 mV at 300 mA cm^{-2} at a relative acceleration rate of 190 *g*. However, cell temperature had a smaller influence on cell voltage and electrode potentials than did electrolyte concentration.

4. Conclusions

Centrifugal fields had a significant effect on the performance of chlor-alkali cells with RuO_2–TiO_2/Ti mesh and DSA anodes, especially with concentrated NaCl solutions at higher temperatures. Under industrial chlor-alkali electrolysis conditions, cell voltage reductions to 600 mV, and anode potential reductions to 360 mV, at 600 mA cm^{-2} were achieved at a relative acceleration rate of 190 *g* in an acidic saturated NaCl solution, compared to those under stationary conditions. The beneficial effect of the centrifugal force is due to an enhancement in mass transport rate and reduction in ohmic resistance by the removal of gas bubbles at an accelerated rate. These factors are being further examined through a mathematical model of the influence of centrifugal fields on electrochemical gas evolution reactions [32]. Overall it is expected that an application of centrifugal acceleration fields in commercial chlor-alkali cells could lead to a substantial reduction in electric energy and, consequently, in the operating cost.

References

1. Published annually in *J. Electrochem. Soc.*
2. D. Pletcher and F.C. Walsh, 'Industrial Electrochemistry' (Chapman & Hall, London, 3rd Edition, 1993), Chapter 3.
3. K. Kinoshita, 'Electrochemical Oxygen Technology' (John Wiley & Sons, New York, 1992), pp. 339–348.
4. D.L. Caldwell, Production of Chlorine, *in* J.O'M. Bockris, B.E. Conway, E. Yeager and R.E. White (Eds), 'Comprehensive Treatise on Electrochemistry', Vol. 2 (Plenum, New York, 1981), pp. 105–166.
5. M.O. Coulter (Ed.), 'Modern Chlor-Alkali Technology', Vol. 1 (Ellis Horwood, Chichester, 1980).
6. C. Jackson (Ed.), 'Modern Chlor-Alkali Technology', Vol. 2 (Ellis Horwood, Chichester, 1983).
7. K. Wall (Ed.), 'Modern Chlor-Alkali Technology', Vol. 3 (Ellis Horwood, Chichester, 1986).
8. N.M. Prout and J.S. Moorhouse (Eds.), 'Modern Chlor-Alkali Technology ', Vol. 4 (Elsevier, London, 1990).
9. T. Wellington (Ed.), 'Modern Chlor-Alkali Technology', Vol. 5 (Elsevier, London, 1990).

10. R. Corry (Ed.), 'Modern Chlor-Alkali Technology', Vol. 6 (Wiley, Chichester, 1995).
11. S. Trasatti and W.E. O'Grady, *in* H. Gerischer and C.W. Tobias (Eds), 'Advances in Electrochemistry & Electrochemical Engineering', Vol. 12 (J. Wiley & Sons, New York, 1981), pp. 177–261.
12. R.D. Varjian, *AIChE Symp. Ser. 204* **77** (1981) 219.
13. M.M. Silver, *AIChE Symp. Ser. 204*, **77** (1981) 234.
14. D.S. Cameron, R.L. Phillips and P.M. Willis, *in* N.M. Prout and J.S. Moorhouse (Eds), 'Modern Chlor-Alkali Technology', Vol. 4 (Elsevier, London, 1990), pp. 95–107.
15. O. de Nora, *Chem.-Ing.-Techn.* **42** (1970) 222.
16. C. Ramshaw, *Heat Recovery Syst. CHP* **13** (1993) 493.
17. D.R. Gabe and F.C. Walsh, *I. Chem. E. Symp. Ser.* **116** (1990) 219.
18. H. Cheng, 'Intensified Electrochemical Processes', PhD thesis, University of Newcastle upon Tyne, Newcastle upon Tyne, UK (1999).
19. M. Shen and Y. Chen, *in* N.M. Prout and J.S. Moorhouse (Eds), 'Modern Chlor-Alkali Technology', Vol. 4 (Elsevier, London, 1990), pp. 149–157.
20. D. Galizzioli, F. Tantardini and S. Trasatti, *J. Appl. Electrochem.* **4** (1974) 57.
21. Y. Katoh, Y. Nishiki and S. Nakamatsu, *J. Appl. Electrochem.* **24** (1994) 489.
22. L.D. Burke and J.F. Healy, *J. Electroanal. Chem.* **101** (1979) 341.
23. H. Vogt, *Electrochim. Acta* **29** (1984) 167.
24. H. Vogt, *Electrochim. Acta* **29** (1984) 175.
25. L. Muller, M. Krenz and R. Landsberg, *J. Electroanal. Chem.* **180** (1984) 453.
26. L.J.J. Janssen and J.G. Hoogland, *Electrochim. Acta* **15** (1970) 1013.
27. H. Vogt, *in* E. Yeager, J.O'M. Bockris, B.E. Conway and S. Sarangapani (Eds), 'Comprehensive Treatise on Electrochemistry', Vol. 6 (Plenum, New York, 1983), pp. 445–489.
28. J.H. Austin, *in* K. Wall (Ed.), 'Modern Chlor-Alkali Technology', Vol. 3 (Ellis Horwood, Chichester, 1986), pp. 131–146.
29. F. Hine, M. Yasuda, T. Noda, T. Yoshida and J. Okuda, *J. Electrochem. Soc.* **126** (1979) 1439.
30. E.A. Kalonovskii, R.U. Bondar and N.N. Meshkova, *Elektrokhimiya* **8** (1972) 1468.
31. A.T. Kuhn and C.J. Mortimer, *J. Appl. Electrochem.* **2** (1972) 283.
32. H. Cheng, K. Scott and C. Ramshaw, submitted to *Chem. Eng. Sci.*
33. A.J. Bard and L.R. Faulkner, 'Electrochemical Methods' (J. Wiley & Sons, New York, 1980), p. 571.